JOURNAL OF CATALYSIS 63, 152–166 (1980)

The Surface Structure of the Active Bismuth Molybdate Catalyst

I. MATSUURA[1], R. SCHUT, AND K. HIRAKAWA[2]

Department of Inorganic Chemistry and Catalysis, University of Technology, Eindhoven, The Netherlands

Received March 12, 1979; revised July 11, 1979

$Bi_2Mo_3O_{12}$ (α), $Bi_2Mo_2O_9$ (β), Bi_2MoO_6 (γ), and mixtures of α and γ were investigated as to their activity for the oxidative dehydrogenation of but-1-ene to butadiene. Pure γ was found to be almost inactive, α was only moderately active, but β and all mixtures of α and γ showed considerable and approximately equal activity. XPS measurements showed the surface of α, β, and γ to have similar Bi/Mo ratios to the bulk. However, for mixtures of α and γ with average ratios $2/3 < Bi/Mo < 2/1$, the Bi/Mo ratio at the surface was found to be approximately equal to 1, decreasing steeply at the Mo-rich side and increasing even more steeply at the Bi-rich edge. The catalytic activity therefore seems to be connected with a surface layer with a Bi/Mo ratio near 1. Adsorption studies on inactive and active catalysts near the Bi/Mo = 2 edge show that B-type adsorption (weak olefin adsorption) is already found on inactive catalyst (stoichiometric γ). A-Type adsorption (strong butadiene adsorption) only becomes observable when a considerable amount of excess MoO_3 is introduced; the amounts adsorbed increase almost linearly with the increase in activity of the catalyst. In infrared and Raman spectroscopic studies, the theoretical positions for the bands related to Mo–O vibrations were determined, using atomic coordinates from the literature and stretching force constants obtained by the application of the Cotton–Wing relation and finally computing the position via a modified Schachtschneider program. The information thus acquired for compounds with known structure was used to analyze the spectra of Bi-molybdates with unknown structure. The results indicate that the active nonstoichiometric catalysts are characterized by the presence of a surface layer on γ. The new bands formed in catalysts containing small amounts of excess MoO_3 were found to be similar to those of β. It is concluded that the surface layer has a structure closely related to that of β. A model of the surface of an active catalyst is given.

INTRODUCTION

The catalytic activity of Bi–molybdates in the oxidation of olefins has been studied by many investigators (*1–4*). Only binary oxides with an atomic ratio in the range $2/3 < Bi/Mo < 2/1$ were found to be active while outside this range there is hardly any activity. The $Bi_2Mo_3O_{12}$ (α), $Bi_2Mo_2O_9$ (β), and Bi_2MoO_6 (γ) are present in catalysts within this range of composition. Opinions vary as to which compound is the active catalyst. Kolchin *et al.* (*5*) observed α and β to have appreciable activity for both oxidation and ammoxidation of propene, while γ displayed only low activity and poor selectivity. On the other hand, Batist *et al.* (*6*) reported γ to be comparable in activity to β for the oxidation of butene to butadiene, while α was only moderately active. Since the three reactions are considered to proceed by similar mechanisms, the conflicting data make it difficult to connect the structure of active sites at the surface unambiguously with a special bulk structure.

The present contribution is an attempt to obtain a better insight into this problem by the application of XPS, ir, and Raman spectroscopy.

EXPERIMENTAL

Catalyst preparation. Bi_2MoO_6 (γ) and $Bi_2Mo_3O_{12}$ (α) were prepared according to a method proposed by Batist *et al.* (*6*). Solid basic bismuth nitrate $BiO(NO_3)$ and molyb-

[1] Present address: Groupe de Physico-Chimie Minérale et de Catalyse, Université Catholique de Louvain, Place Croix du Sud 1, 1348 Louvain-la-Neuve, Belgium.

[2] Present address: Asahi Chemical Industry Co. Ltd., Tokyo, Japan.

0021-9517/80/050152-15$02.00/0

dic acid H_2MoO_4 were powdered, slurried in water, and boiled under stirring for 16 hr. Thereafter, the solid materials were filtered and dried. The initial ratio of Bi to Mo was 2 : 1 for the synthesis of γ and 1 : 5 for α. In order to remove the excess of MoO_3 for the latter case, the calcined sample was washed with a diluted ammonia solution. $Bi_2Mo_2O_9$ (β) was prepared by coprecipitation from bismuth nitrate $Bi(NO_3)_3 \cdot 5H_2O$ and ammonium hepta-molybdate $(NH_4)_6Mo_7O_{27} \cdot 4H_2O$, as described by Batist *et al.* (*6*). The samples of the various oxides were calcined at 500°C for 4 hr. The oxides will be referred to as compounds α, β, and γ as a convenient short notation.

Catalysts with other atomic ratios of Bi and Mo, $0.58 \leqq Bi/Mo \leqq 2.04$, were also prepared, using the same method as for the compound γ. In this paper, they will be called "multiphase" samples, although X-ray analysis sometimes showed only the presence of one compound. The atomic ratio of Bi to Mo in these samples was determined by means of atomic absorption spectrometric analysis.

We also prepared some catalysts by impregnating stoichiometric Bi_2MoO_6 (γ) with MoO_3 or Bi_2O_3 ("impregnated" samples). Previously prepared γ samples were slurried in a solution of H_2MoO_4 or $Bi(NO_3)_3 \cdot 5H_2O$ of the appropriate concentration. After evaporation under stirring, the solids were calcined at 520°C for 2 hr.

X-Ray analysis showed only the expected phase in the α and γ compounds. For compound β, small amounts of α and γ were present. In the multiphase samples, only a mixture of compounds α and γ were found, without compound β being observable. Samples near 2/1, with compositions situated between an excess of 4% Bi to an excess of 8% Mo, showed only the lines of the γ-phase.

The surface areas of the various samples are plotted versus the atomic ratio of Bi/Mo in Fig. 1. Densities also shown in this figure are determined pycnometrically with carbon tetrachloride. The values of the densities of the three compounds are close to the densities calculated from the unit cell dimension of the crystal structure.

	Obs	Calcd
Bi_2MoO_6 (γ)	7.8	8.0 (7)
$Bi_2Mo_2O_9$ (β)	6.5	6.6 (8)
$Bi_2Mo_3O_{12}$ (α)	6.0	6.2 (9)

It is noteworthy that multiphase samples usually had higher surface areas and lower densities than the pure compounds.

Catalyst activity measurements. The catalytic activity of the various samples for the oxidation of but-1-ene to butadiene was determined for a range of temperatures from 350°C upwards. The apparatus, procedure, gas chromatographic analysis, and the method of calculation were given earlier by Batist *et al.* (*10*). In each experiment sample weights of unit surface area were used, the gas flows were 20 $cm^3\ min^{-1}$ of butene and 100 $cm^3\ min^{-1}$ of artificial air.

But-1-ene and butadiene adsorption measurements. A conventional vacuum apparatus equipped with a quartz adsorption cell was used for isotherm measurements. The measurements were performed over a range of pressures from 10^{-3} to 10 Torr and a range of temperatures from 0 to 200°C. The adsorption method was described elsewhere (*11*).

XPS measurements. X-Ray photoelectron spectroscopy was performed using an

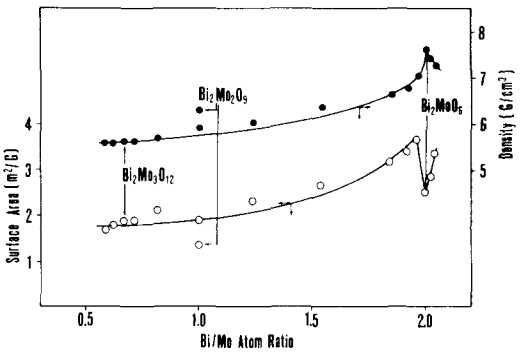

FIG. 1. Surface areas and bulk densities of various "multiphase" samples and "compounds" of Bi-molybdates as a function of composition.

AEI ES 200 spectrometer with Mg$K\alpha$. The power supply was run at 12 kV and 15 mA, the spectra being collected with a PPDS computer and stored in a 32 K disc. The powdered samples were mounted on adhesive tape.

Infrared and raman spectra measurements. The ir spectra of samples were recorded with a Grubb Parsons spectrometer MK-3 in the range of 1250–400 cm^{-1} and a Hitachi model EP 1-92 in the range of 700–200 cm^{-1}, using the conventional KBr disk techniques. The Raman spectra of powders from 1250 to 0 cm^{-1} were obtained using a Varian carey-82 with an Ar laser (5145 Å). Samples were either measured on a rotating disk or in glass capillary tubes; no essential difference was observed between spectra observed by the two methods.

EXPERIMENTAL RESULTS

Catalytic activity measurements. Figure 2 shows the activities of the catalysts. For all catalysts, the selectivity to butadiene was found to be higher than 95% over the whole temperature range. The compound γ was found to be only weakly active. Multiphase samples around 2/1 with a small excess of Mo are fully active, while those with a small excess of Bi are entirely inactive. The decline at the 2/1 edge appears to be very sharp. The compound α is only moderately active, but a slight excess of Bi brings the sample to an activity level comparable to that of the compound β and all samples with $0.8 \leq Bi/Mo \leq 1.92$ show similar activities at temperatures higher than 440°C. However, at temperatures lower than 410°C, the activities decrease with decreasing of Bi/Mo ratio.

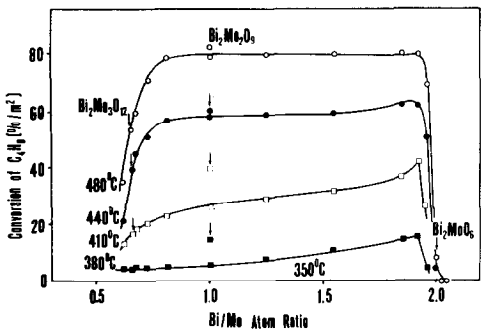

FIG. 2. Conversion of but-1-ene (per unit surface area) as a function of composition for "multiphase" samples and "compounds" of Bi-molybdates.

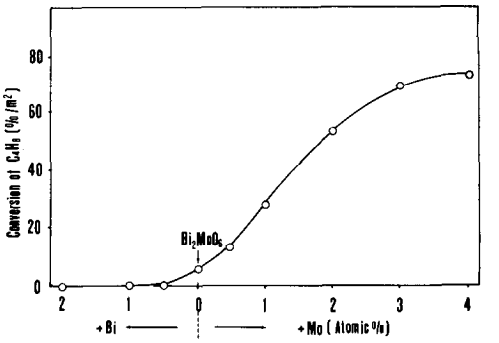

FIG. 3. Conversion of but-1-ene (per unit surface area at 440°C) as a function of addition of MoO_3 or Bi_2O_3 on stoichiometric Bi_2MoO_6 (impregnated samples).

The activities of the impregnated samples at 440°C are shown in Fig. 3. The results show equally spectacular changes as found with the multiphase samples in the corresponding range. Addition of 4% MoO_3 (atomic percent with respect to Mo, i.e., $Bi_2MoO_6 \rightarrow Bi_2Mo_{1.04}O_{6.12}$) causes an activity increase by a factor of at least 10. Since, in impregnation, the excess MoO_3 may be assumed to be deposited at the surface, it might be surmised that the multiphase samples also have an excess Mo at the surface.

Adsorption measurements. The adsorption of but-1-ene over all "impregnated" samples is found to be always weak, fast, and reversible. A small excess Bi in the 2/1 surface shows an associative chemisorption with a rather weak heat of adsorption at 25 kJ $mole^{-1}$, similar to that reported earlier by one of us on Bi_2O_3 (*11*). Stoichiometric Bi_2MoO_6 (γ) has a different type of adsorption with a higher heat of adsorption at 46 kJ $mole^{-1}$ and the characteristics of a dissociative adsorption. This adsorption is closely similar to that described earlier by one of us as B-type adsorption (*11*). Addition of MoO_3 shows no change of the ad-

TABLE 1

Adsorption Data of But-1-ene and Butadiene on Impregnated Samples

Catalyst	Composition	Type of isotherm	V_m (cm^3m^{-2})	Log P_0^0 (mm Hg)	Heat of adsorption Q (kJ mol^{-1})
Bi_2MoO_6	C_4H_8	DS(w)[a]	0.141	8.9	42.2
	C_4H_6	DS(W)	0.138	6.6	41.9
		Strong ads.	no obs.		
+ 1% Bi_2O_3	C_4H_8	SS(w)[b]	0.106	4.7	25.2
	C_4H_6	SS(w)	0.108	4.7	23.1
		Strong ads.	no obs.		
+ 1% MoO_3	C_4H_8	DS(w)	0.133	9.2	46.2
	C_4H_6	DS(w)	0.135	6.6	42.1
		Strong ads.	0.013		
+ 2% MoO_3	C_4H_8	DS(w)	0.130	9.5	46.2
	C_4H_6	DS(w)	0.130	6.9	42.0
		Strong ads.	0.023		
+ 4% MoO_3	C_4H_8	DS(w)	0.116	9.5	46.2
	C_4H_6	DS(w)	0.118	6.9	41.6
		Strong ads.	0.032		

[a] DS, dual-site adsorption.
[b] SS, single-site adsorption.

sorption parameters but decreases the surface concentration. The activated and strong desorption of butadiene, A-type adsorption, described in the earlier paper (*11*), is not present on Bi-enriched or stoichiometric Bi_2MoO_6 (γ). It only becomes observable when a considerable amount of excess MoO_3 is introduced. The adsorption parameters for the Langmuir–Hinshelwood isotherm are given in Table 1.

XPS measurements. Figure 4 shows the XPS spectra of compounds α, β, and γ and of two multiphase samples near the 2/1 edge but with a slight excess of Mo or Bi. To calculate the Bi/Mo atomic ratio at the surface we used the method proposed by Carter *et al.* (*12*) who applied the photoelectron cross sections of Scofield (*13*) for Al$K\alpha$ or Mg$K\alpha$ radiation. The relative intensity N for two different photoelectron peaks from the same samples is given as

$$N_1/N_2 = \sigma_1 n_1 \lambda_1 S_1 / \sigma_2 n_2 \lambda_2 S_2, \qquad (1)$$

where σ is the photoelectron cross section for a given subshell of a given element, n is the concentration of atoms per unit volume, S is the spectrometer factor, and λ is the mean free path. Assuming that the ratio of the S factor is not dependent on the energy

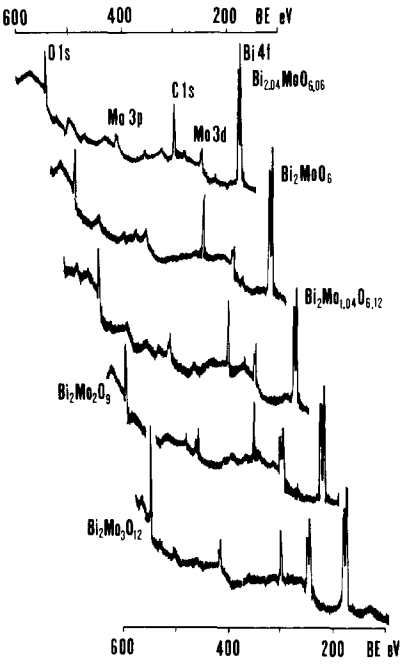

FIG. 4. XPS spectra of "compound" Bi-molybdates and "multiphase" samples near the 2/1 edge.

and that the mean free paths can be approximately fitted by the equation $\lambda \propto E^{1/2}$, we arrive (for $n_1 = n_2$) at the following relation:

$$N_1/N_2 = \sigma_1(h\nu - E_{B1})^{1/2}/\sigma_2(h\nu - E_{B2})^{1/2}, \quad (2)$$

where E_B is the energy of the level under investigation and $h\nu$ is the energy of the radiation quanta.

The value of the relative intensity ratio of N_{Bi}/N_{Mo} is found to be 2.5 from Eq. (2), taking the value of $\sigma_{Bi,4f(7/2)}$ and $\sigma_{Mo,3d(5/2)}$ to be respectively 14.0 and 5.77 as calculated by Scofield (*13*), and $E_{B,Bi,4f(7/2)}$ and $E_{B,Mo,3d(5/2)}$ as equal to respectively 159 and 232 eV.

Comparing the Bi/Mo ratios thus predicted with the experimental values for the compounds α, β, and γ, there is excellent agreement between bulk compositions and surface compositions, as shown in Fig. 5. However, for all multiphase samples the Bi/Mo ratio in the catalytically active range is found to be near 1, similar to the value of the compound β (see Fig. 5).

Infrared and raman spectra. The ir bands of compound γ and 2/1 with excess MoO_3 are shown in Fig. 6a. The band positions of the stoichiometric compound are similar to those given in the literature (*14*). Above 600 cm^{-1}, the "excess MoO_3" samples exhibit a new set of weak bands superimposed upon the existing ones. There is a sharp, weak band at 832 cm^{-1}, while the main 735-

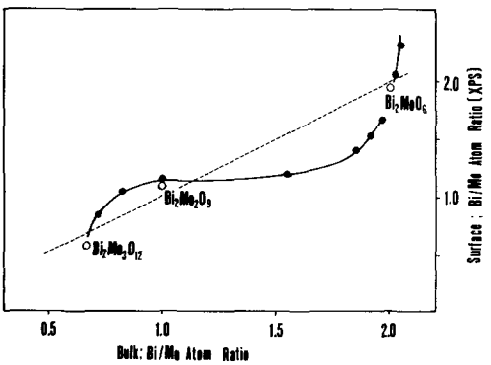

FIG. 5. Atomic ratio of Bi/Mo at surface from XPS analysis as a function of bulk composition for "multiphase" samples and "compound" Bi-molybdates.

cm^{-1} band broadens considerably with a shoulder at 760 cm^{-1} as shown in Fig. 7.

The Raman spectrum of compound γ (Fig. 6a) shows three bands at 848, 799, and 715 cm^{-1}, of which the second is strong. Between 200 and 400 cm^{-1}, there are two moderately strong bands at 325 and 272 cm^{-1} with some smaller bands. The range of 400 to 600 cm^{-1} is practically empty. Excess MoO_3 causes the appearance of new sharp bands at 886 cm^{-1} and two weak shoulders at 809 and 782 cm^{-1}. Figure 7 shows increasing intensity of these new bands with addition of MoO_3 in Bi_2MoO_6 (γ).

Compound γ heated at 645°C (X-ray diagram shows the Blasse phase, γ') are more complicated than those of koechlinite (γ) over the whole range: there are at least nine bands in the ir and Raman spectra above 600 cm^{-1} (see Fig. 6b).

The spectra of compound β are shown in Fig. 6c. The ir spectra show a sharp band at 890 cm^{-1} and a much stronger and broader band between 650 and 850 cm^{-1}; it is also possible to observe shoulders (840, 710 cm^{-1}) and peaks (800, 770, 740 cm^{-1}). The Raman spectra show the presence of two strong bands (892, 793 cm^{-1}) with two weaker bands at 845 and 715 cm^{-1}.

The band positions of the complicated spectrum for compound α are similar to those in the literature (*15*). The positions of ir and Raman bands observed for the compounds are summarized in Table 2.

A short survey of the results for other compounds follows below (band positions in cm^{-1}):

MoO_3: 990(s), 875(s), 815(w), 640(sh), 620(s), 510(vw), 485(vw), 375(s), 358(vw), 350(vw), 310(s), 305(sh), 280(sh), 240(sh).

Bi_2O_3: no ir bands above 600 cm^{-1}; below 600 cm^{-1} broad bands on strong background bands at 545, 510, 450(sh), 430, 340, and 270.

$BiO(NO_3)$: band in ir at 1380 (s), 835, and 820(w) presumably NO_3^- (ν_3, ν_2, and ν_4), 540(s,b), 380(s,b), and 275(s,b).

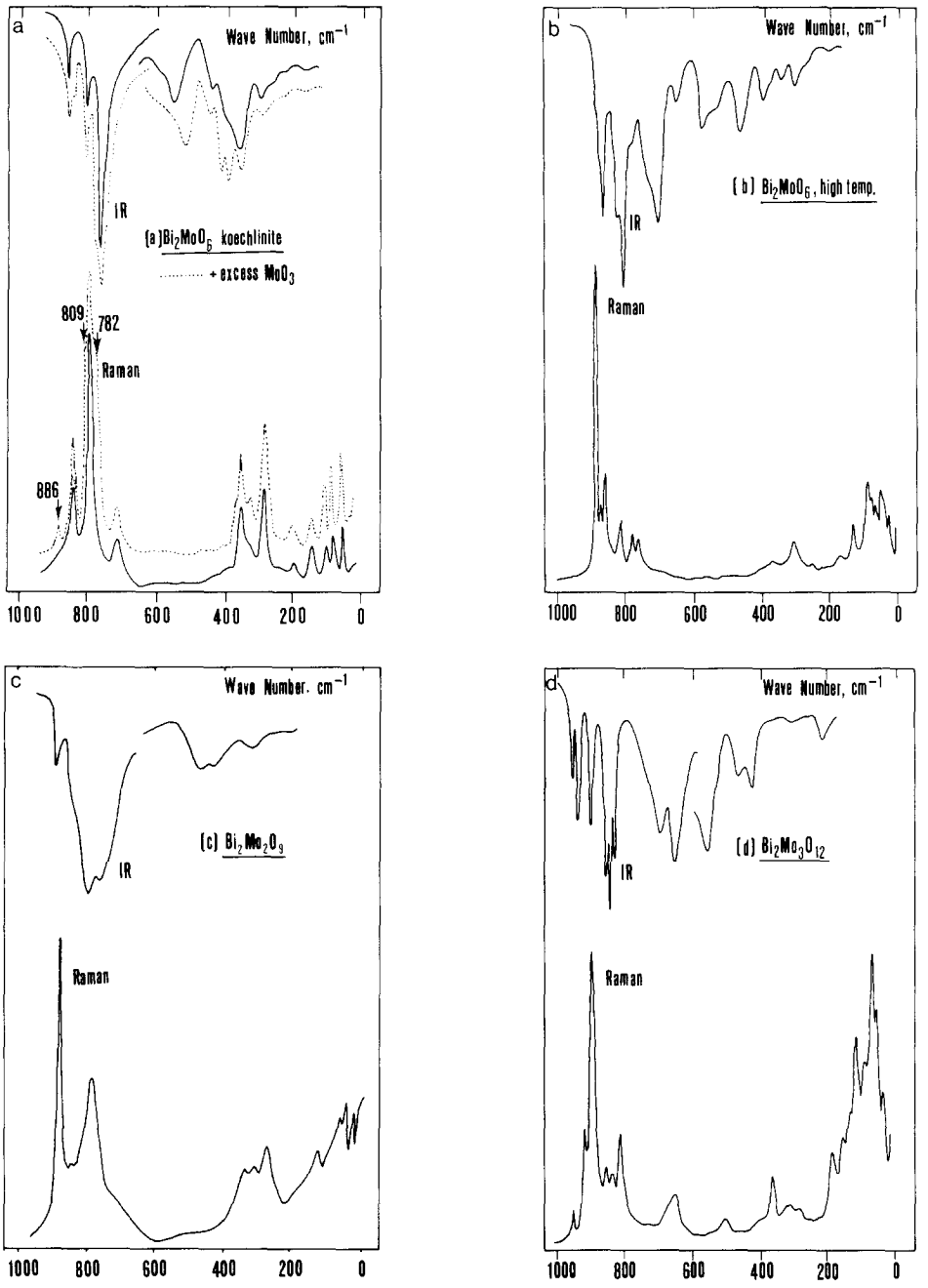

FIG. 6. Infrared and Raman spectra for Bi-molybdates; (a) Bi_2MoO_6 (γ) (b) Bi_2MoO_6 (γ'), (c) $Bi_2Mo_2O_9$ (β), and (d) $Bi_2Mo_3O_{12}$ (α).

DISCUSSION

Interpretation of ir and raman spectra. The crystal structures of the bismuth molybdates have been studied with precision by Van den Elzen and Rieck (*16–18*). Two structures, viz., those of Bi_2MoO_6 (γ) and $Bi_2Mo_3O_{12}$ (α), are now known with considerable accuracy from X-ray diffraction analysis. An "outline model" was given for

TABLE 2

Infrared and Raman Spectra of Bismuth Molybdates

Bi_2MoO_6 (γ)		Bi_2MoO_6 + 4% MoO_3 (extra bands)		Bi_2MoO_6 (γ')		$Bi_2Mo_2O_9$ (β)		$Bi_2Mo_3O_{12}$ (α)	
ir	Raman	ir	Raman	ir	Raman	ir	Raman	ir	Raman
842_m	843_{30}		886_{16}	890_{sh}	892_{100}	890_m	892_{100}	948_m	955_{10}
798_w	799_{100}	832_{sh}		880_{sh}	883_{30}	840_{sh}	845_{30}	931_m	919_{30}
735_{vs}	715_{15}		809_{sh}	868_{vs}	864_{41}	800_s	793_{60}	902_m	897_{82}
600_w		760_{sh}	782_{sh}		851_{23}	770_s		860_s	853_{20}
		710_w		825_m	822_{37}	740_m	715_{10}	847_s	836_{18}
				810_{vs}		710_{sh}		830_m	811_{28}
				780_w	787_{25}			715_m	
					770_{29}			670_s	654_{12}
				740_m					
				710_s	695_{25}				
				645_m					
570_m		545 shifted		562_m		500_{sh}		570_m	
		from 570		527_w				550_{sh}	
450_m				467_w		473_m		470_m	
						446_m		440_m	
								415_{sh}	
408_m		408_{st}		391_w	399_9	409_m		392_m	
390_{sh}	399_5	390_{st}		380_w	375_{13}	392_w		350_w	360_{18}
352_s	354_9	358_{st}		335_w	359_{10}	362_m	356_{15}	314_m	317_9
304_m	326_{15}			300_w	315_{25}	325_{vw}	323_{16}	303_{vw}	302_3
287_w	295_{13}			290_{vw}	303_{27}	275_m	286_{21}	276_{vw}	282_8
277_{vw}	278_{18}				258_{16}	266_w	260_5	262_{vw}	248_5
268_{vw}					226_9		180_2		
248_{vw}					206_9				
	194_5								

TABLE 3

Crystallographic Data for Bismuth Molybdates

	Bi_2MoO_6 Koechlinite (γ)	Blasse (γ')	$Bi_2Mo_2O_9$ (β)	$Bi_2Mo_3O_{12}$ (α)
Crystal system	Orthorhombic	Orthorhombic	Orthorhombic	Orthorhombic
Monoclinic				
Space group	*Pca* 2_1	*P* $2_1/c$	*P* $2_1/c$	*P* $2_1/c$
Coordination of Mo^{6+}	Distorted octahedral	Tetrahedral	Trigonal-bipyramidal or tetrahedral	Trigonal-bipyramidal or distorted tetrahedral
Mo–O bond length (Å)	Bi_2MoO_6 (γ)	$Bi_2Mo_3O_{12}$ (α)		
	γ-	α_1-	α_2-	α_3-
	$Mo–O_1$ 1.86	$Mo_1–O_4$ 1.69	$Mo_2–O_1$ 1.72	$Mo_3–O_{12}$ 1.68
	$–O_4$ 2.24	$–O_5$ 1.72	$–O_9$ 1.73	$–O_{11}$ 1.78
	$–O_4$ 1.76	$–O_2$ 1.85	$–O_6$ 1.86	$–O_8$ 1.86
	$–O_5$ 2.24	$–O_{10}$ 1.92	$–O_3$ 1.89	$–O_7$ 1.87
	$–O_5$ 1.75	$–O_{10}$ 2.25	$–O_8$ 2.13	$–O_6$ 2.30
	$–O_6$ 1.93			

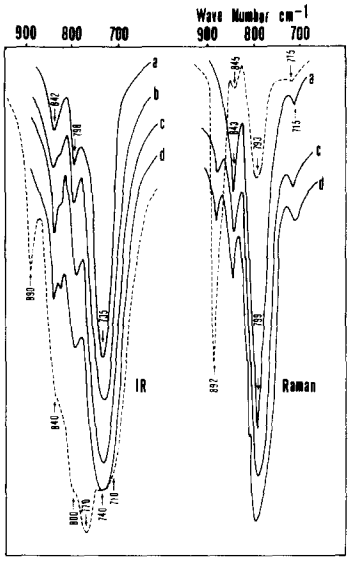

FIG. 7. Infrared and Raman spectra for "impregnated" samples; (a) stoichiometric Bi_2MoO_6 (γ), (b) 1 atom% of excess MoO_3, (c) 2 atom%, and (d) 4 atom%. Dashed line indicates $Bi_2Mo_2O_9$ (β).

$Bi_2Mo_2O_9$ (β) for which only powder diagrams could be obtained. Crystallographic data are given in Table 3.

A common feature of all these structures is the existence of MoO_n and BiO_m polygons with several, but not necessarily all, oxygen shared. An extensive literature concerns the spectra on MoO_n, with n varying between 4 and 6. It is usually assumed that $n = 6$ (octahedral) for Bi_2MoO_6 (γ) and $n = 5$ (trigonal bipyramidal) for $Bi_2Mo_3O_{12}$ (α). However, the inspection of the structures reveals that, for both cases, there are two "short" bonds and two "intermediate" bonds, with in addition, for compound γ, two "long" bonds, and for compound α, one "long" bond. The long bonds in both cases refer to an oxygen bonded with a "short" bond to a neighboring Mo (see Table 3). It therefore appears appropriate to assume that all Mo–oxygen polygons encountered here are derived from tetrahedral MoO_4. The particular type of distortion can then be considered characteristic for the crystal structure. The structure of the "surface layer", of different form from that of the bulk, may, if circumstances permit, be guessed from the MoO_4 spectra. A more extensive analysis of the spectra from compounds with known structure is thus necessary.

A tetrahedral group (T_d) has four vibrational modes, $\nu_1(A)$, $\nu_2(E)$, $\nu_3(F_2)$, and $\nu_4(F_2)$. All are Raman active, while only the triply degenerative modes are ir active. A complete lifting of the degeneracies would give a system of nine bands. Since $\nu_1(A)$ and $\nu_3(F_2)$ are intrinsically connected with stretching and $\nu_2(E)$ and $\nu_4(F_2)$ with bending modes, it may be expected that every Mo–O_4 configuration produces two groups of bands, positioned at different parts of the spectrum.

Busey and Keller (*19*) give information about the position of the two groups. Powdered Na_2MoO_4 has four Raman bands at 892(vs), 808(s), 381(m), and 303(m) cm^{-1}, while there are two ir bands at 838 and 325 cm^{-1}. This indicates that the stretching modes are around 800 cm^{-1} and the bending modes between 300 and 400 cm^{-1}. Only the former are therefore useful to us, since the bending mode range for our system is probably overlapped by Bi–O bands. Somewhat closer to our system is $PbMoO_4$ with the scheelite structure, and all Mo–O bands equal to 1.772 Å (*20*). Tarte and Liegeois-Duyckaerts (*21*) found four ir bands (786, 374, 307, 242 cm^{-1}) and six Raman bands (869, 766, 743, 357, 350, and 317 cm^{-1}). It is noteworthy that, contrary to Bi-molybdates, the 400 to 600-cm^{-1} range is empty, in good agreement with our assumption that bands in this range belong to Bi–O vibrations. It seems clear that there is sufficient evidence to accept that bands around 550 cm^{-1} belong to this category. These bands are observable in $BiO(NO_3)$ and in BiOX with X being Cl, Br, or I (*22*). Also, Hulett and Thornton (*23*) investigated Bi troponolate complexes in which the troponolate anion (Tr) is a bidendate ligand. They found for $BiTr_2Cl$ bands at 514 and 580 cm^{-1} while $BiTr_3$ has a band at 570 cm^{-1}.

According to the X-ray structure, compound γ has only one type of MoO_4 unit (γ)

and there should be only four bands around 800 cm^{-1}. This is what is observed, although it is somewhat difficult to locate the position of the fourth band that could be either the very weak 600 cm^{-1} or the somewhat stronger 570 cm^{-1} band. In agreement with the presence of three different MoO_4 groups (α_1, α_2, and α_3), the higher range of the compound α spectra are very complicated with at least nine bands. A more extensive analysis is therefore necessary before the spectra can be completely explained.

In order to do so, we used the G-F matrix method. Atomic coordinates and bond lengths were derived from the X-ray structural analysis of Van den Elzen and Rieck (*16, 17*) (see Table 3). Stretching force constants were derived from the Cotton–Wing relation (*24*) between Mo–O distance and stretching force constants. Stretching–stretching interaction constants, bending force constants, and bending–bending interaction constants were taken equal to those of tetrahedral MoO_4 (0.55, 0.35, and 0.02 m dyn/Å (*25*)). The computer program used was written by Bril and Vogel (*26, 27*) and is an extension of the Schachtschneider NCA program. Initial results were promising enough to warrant further refinement by slightly modifying the Cotton–Wing relation. The final results are given in Table 4, where they are confronted with the experimental results. There is a satisfactory agreement between predicted and observed band positions. Also, they clearly show that the range 600–400 cm^{-1} is now empty, the bending modes being situated in the range 375–200 cm^{-1}. The various experimentally observed bands can now be properly assigned to the various MoO_4 groups, as indicated in Table 4.

The agreement between prediction based on the tetrahedral model and experiment shows conclusively that the MoO_4 model is entirely sufficient to describe the spectra. It is therefore doubtful whether evidence from ir and Raman spectroscopy can be used to make a distinction between "octahedral" or "tetrahedral" surrounding of the molybdenum. It does, however, allow the recognition of a greater or lesser degree

TABLE 4

Calculated Band Positions for MoO_4 of Bi_2MoO_6 (γ) and $Bi_2Mo_3O_{12}$ (α) and Comparisons with Observed Bands (cm^{-1})

MoO_4 (γ) of Bi_2MoO_6 (γ)			$Bi_2Mo_3O_{12}$ (α)					
Calculated			$MoO_4(\alpha_1)$	MoO_4 (α_2)	$MoO_4(\alpha_3)$			
	Observed					Observed		Assignment
	ir	Raman		Calculated		ir	Raman	
865	842	848			933	948	955	α_3
780	798	799	921			931	919	α_1
693	735	715		886		906	897	α_2
613	600		849			860	853	α_1
				822		847	836	α_2
					796	830	811	α_3
			703	690	690	715		$\alpha_{1,2,3}$
			651	665	680	670	654	$\alpha_{1,2,3}$
376	375	399	345	343	341	350	360	
355	354	354	336	340	334	314	317	
337	304	326	335	336	330	303	302	
287	287	293	295	292	297	276	282	
196		194	295	249	263	262	248	

of distortion of the pseudotetrahedral configuration. For instance, taking the accepted structure of γ and α, as determined by X-ray diffraction, one can predict that the former should have a Mo–O–Bi mode of vibration near 600 cm^{-1} but not the latter. Since both have a 570-cm^{-1} band but only the former has a band (very weak), only this latter band should be attributed to the MoO_4 stretching mode. The quantitative agreement (theory, 613; experiment, 600 cm^{-1}) confirms this assignment.

Let us now discuss the spectra of Bi-molybdates for which the structure is only approximately known (γ', β). For the γ'-Bi_2MoO_6, Blasse (*28*) considers its structure to be similar to that of koechlinite (γ) except for the arrangement in the MoO_2-layer. He suggests this to consist of separate MoO_4-groups. The complexity of the spectra of γ' indicates the presence of at least two, but possibly three, different MoO_4 configurations. The prediction of Blasse (*28*) that the structure is similar to that of koechlinite (γ) is therefore not entirely acceptable. In fact, the γ'-spectrum is more similar, although not identical, to that of $Bi_2Mo_3O_{12}$ (α).

Van den Elzen and Rieck (*18*), in their outline of a model for the $Bi_2Mo_2O_9$ (β) structure, consider all MoO_4-units as equivalent; we showed above that there might be two different types of MoO_4, although the extent to which they are different cannot be specified. Supposing, according to their model, that compound β contains building elements such as are present in compound γ and α, then the two MoO_4 structures might resemble γ-MoO_4 and one of the α-MoO_4 units. Indeed, three of the four γ-MoO_4 bands (840, 790, and 740 cm^{-1}) are observable in the spectra of β, while the fourth band at 600 cm^{-1} is very weak. So we propose that there is a γ-set similar to the β_1-set. It is also remarkable that not only the position but also the ir and Raman intensities of the genuine γ-set and that assumed in the β_1-set agree, the 790 to 800-cm^{-1} band being strong in Raman but weak in ir while the 735-cm^{-1} band is strong in ir with no Raman band observable at this point. The remaining bands, 890(R), 770(ir), and 715(ir) with 840-cm^{-1} (R, ir) band presumed to make up the β_2-set, have some similarity with the α_2-set in $Bi_2Mo_3O_{12}$ (α) but the 770-cm^{-1} band is absent in the compound α.

Our proposal is similar to that of Gryzbowska *et al.* (*29*) and of Mitchell and Trifirò (*30*), except for the fact that they consider $Bi_2Mo_2O_9$ (β) to have tetrahedral and octahedral Mo which we choose to be more specific by insisting that the tetrahedral surrounding is actually a distorted trigonal bipyramidal arrangement (α_2-set) and "octahedral" Mo is strongly distorted, similar to that of the γ-set.

We now compare the positions of incipient bands formed by the introduction of small amounts of MoO_3 in Bi_2MoO_6 (γ) with those of the bands of the compounds. We start with the set of extra bands in the range above 600 cm^{-1} (see Table 2 and Fig. 7, where the ir and Raman bands of $Bi_2Mo_2O_9$ (β) are confronted with those of the impregnated samples). It is obvious that there is no correspondence with the band positions for the MoO_3-set. There is, however, a distinct similarity with the β_2-set. Two strong bands for this compound, the strong 892-cm^{-1} Raman band and the massive 770-cm^{-1} ir band, coincide with a tiny Raman peak at 886 cm^{-1} and a rather strong shoulder around 760 cm^{-1} (ir) on the γ-band. A small but distinct shoulder at 832 cm^{-1} (ir) in the extra set was not traced in the β-spectrum, but could have been overlooked because it fused with the 840-cm^{-1} band ($\gamma = \beta_1$). If so, the complete β_2-set would be 890–892, 832, 770, 710–715, and 473 cm^{-1}. The extra set could not be derived from $Bi_2Mo_3O_{12}$, because the α_1 and α_3 bands are completely lacking and α_2, although slightly resembling β_2, is definitely different as remarked before. We therefore conclude that the incipient set of bands is that of a surface layer with a structure closely resembling that of $Bi_2Mo_2O_9$; the set is very similar to

β_2 while $\beta_1 = \gamma$ remains hidden by the more massive Bi_2MoO_6 spectrum.

Next we turn to the change occurring in the Bi_2MoO_6 spectra below 600 cm^{-1} (see Fig. 6a and Table 2). These spectra are different in character from those considered above. Above 600 cm^{-1}, we find the formation of new bands of low intensity next to the more massive bands of the mother compound. We also observe bands already present in the Bi_2MoO_6 spectra that shift positions and become more intense. The general impression is that of an increase in regularity. While the new bands above 600 cm^{-1} could be assigned to surface layers, the changes below 600 cm^{-1} are undoubtedly connected with changes in the bulk, certainly an unusual phenomenon considering the small amounts of MoO_3 incorporated. Even more surprising is that incorporation of more substantial amounts, up to 30%, does not lead to further changes.

The changes occur in two regions, viz.:

(i) Betwen 570 and 500 cm^{-1}, i.e., where the Bi–O bands are supposedly situated. The weak 570-cm^{-1} band moves to 545 cm^{-1} and becomes more intense. Hulett and Thornton (*23*) observe similar shifts in passing from $BiTr_2{}^+Cl^-$ to $BiTr_3$ (from 514 to 495 cm^{-1}). They ascribe this to an increase in coordination number from 4 to 6.

(ii) In the Mo–O bending vibration range at 400–200 cm^{-1}, a rather broad and irregular band in the ir below 410 cm^{-1} grows to a system of three equally intense bands at 410, 390, and 358 cm^{-1}. Similarly, in the Raman we now find three quite distinct bands at 354, 326, and 295 cm^{-1}.

The following tentative explanation is offered to account for the phenomena. We start from the assumption that samples of stoichiometric Bi_2MoO_6 contain defects of a type in which Mo and Bi are in the wrong cation positions. Interdiffusion of cations would eliminate the defects, but this could be supposed a difficult process, since there are no cation vacancies. However, once vacancies are produced by the incorporation of small amounts of Mo, the defect lattice can relax, because cations can now migrate. In other words, the spectra produced after Mo incorporation are those that actually belong to the defect-free Bi_2MoO_6. The ir group might be related to the $\nu_4(F_{1u})$ bending mode of O_h (only infrared active) and the Raman group to $\nu_5(F_{2g})$.

Introduction of cation vacancies by Mo incorporation can be supposed to "catalyze" other phase transitions. We found indeed that the koechlinite to Blasse phase transition occurs at temperatures appreciably lower for Bi_2MoO_6 + small amounts of MoO_3 (580°C) than for stoichiometric Bi_2MoO_6 (640°C).

Surface structure and catalytic activity. The combined evidence of XPS and ir and Raman spectroscopy strongly supports the hypothesis that the catalytic activity of Bi-molybdate system resides in "surface domains" that may be different in structure and composition from the bulk. Here we postulate that the "surface domains" are similar in structure and composition to $Bi_2Mo_2O_9$ (β). The following arguments underline this hypothesis:

(1) While compound γ (stoichiometric) is almost inactive and compound α has low activity, all mixtures of the two in the range $2/3 < Bi/Mo < 2/1$ are very active and have an activity similar to that of compound β.

(2) Even relatively small amounts of MoO_3 in excess of the stoichiometric ratio suffice to bring the catalyst to maximal activity: $Bi_2Mo_{1.04}O_{6.12}$ is just as active as compound β.

(3) XPS data show the existence of a surface layer with a composition different from that of the bulk phase, the Bi/Mo ratio at the surface in the high-activity range being almost constant at a level near 1.

(4) The ir and Raman spectra of catalysts such as $Bi_2Mo_{1.04}O_{6.12}$ show a new, weak set of bands in the stretching mode region of Mo–O vibrations. This set is different from that of pure MoO_3; this shows that superficial MoO_3 has reacted with the underlying Bi_2MoO_6 (γ). This set of bands is

similar to one of the sets (β_2) that can be observed in the spectrum of β.

(5) Since the other band system of this compound (β_1) is akin to that of compound γ, a layer of β on γ would only show the β_2-set superposed on the γ-set, as was observed.

For the structure of $Bi_2Mo_2O_9$ (β), the model (*18*) proposed is a combination of elements derived from the Scheelite and from the koechlinite (γ) structure. The Scheelite-derived contribution is a stacking of four Mo, in a square pattern, bound together by Bi positioned on the axis passing through the centers of the squares and half-way between two groups of four Mo ("Mo_4"). It is assumed that the "Mo_4" arrangement represents Mo_4O_{16} clusters bonded together by bridging oxygens, as in the Mo_2O_8 groups in compound α. The particular Bi-cations (Bi^I) are therefore surrounded by eight MoO_4 units, as is Pb^{2+} in $PbMoO_4$, the difference being that the distance between the MoO_4 units is smaller in two crystallographic directions (x and z). A typical koechlinite (γ) building element is given by the linear rows of oxygens, running parallel to the (Mo_4O_{16})–Bi–(Mo_4O_{16}) axis. These oxygens are only connected to Bi-cations and are similar to ribbons of $Bi_2^{III}O$ cut out from the Bi_2O_2-planes in koechlinite, while the Bi^{III}-cations are further linked to the oxygens of the Mo_4O_{16}-groups. A noteworthy detail is that not all these Bi-sites are filled, one in every four sites being empty. The model might be summarized by writing it as

$$Bi^I(Bi_3^{III}\phi_cO_2)(Mo_4O_{16}),$$

ϕ_c being the empty cation site.

As we discussed earlier, the structure of β thus appears more closely related to the structure of γ than believed so far. Figures 8a and b suggest a method to illustrate the structural relation. Figure 8b gives cation and cation vacancy positions in the (010) plane of the β structure (*18*). The crystal planes (101) perpendicular to this cation plane can now be related to the (Bi_2O_2) and (MoO_2) planes in compound γ as shown in Fig. 8a. To go from Fig. 8a to b, pairs of Bi-cations have to be replaced by one Mo and one cation vacancy, but there is simultaneously some reshuffling of cations according to the scheme

$$(Bi_2)(Mo) \rightarrow (BiMo_{2/3}\phi_{1/3})(Mo_{2/3}Bi_{1/3}),$$

i.e., Bi-cations are replaced by Mo in the Bi_2O_2 layer but simultaneously some Mo has been replaced by Bi in the MoO_2 layer. If we assume the oxygen positions to remain similar to those in $Bi_2MoO_6(\gamma)$ we arrive at Fig. 8c. It is then obvious that there are two different oxygen surroundings of Mo, one equal to the γ-surrounding, the other a new one in the Bi_2O_2-derived layer. Of course, since the γ-structure chosen as the starting position represents a simplification of the more distorted real structure, it is probable that similar distortions will occur in the β-structure. However, the model is adequate to expalin the spectral observation as to its essential points.

A sample with a bulk composition Bi/Mo = 1.96 has sufficient excess MoO_3 to cover the entire Bi_2MoO_6 surface with a layer of MoO_3. XPS data show, however, that the surface Bi/Mo ratio remains as high as 1.5. Noble-gas ion reflexion mass spectrometry (NIRMS) studies carried out by courtesy of Professor H. H. Brongersma also indicate an almost equal ratio (Bi/Mo = 1.6). According to calculations based on the experi-

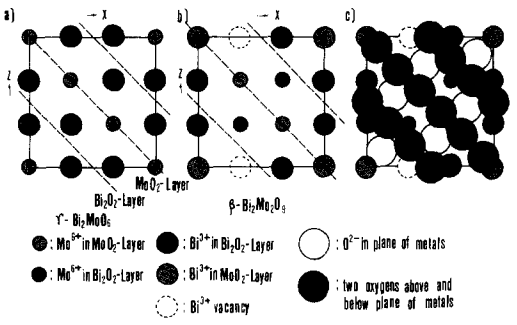

FIG. 8. Cation positions for (a) Bi_2MoO_6 (101) plane, (b) $Bi_2Mo_2O_9$ (010) plane, and (c) modified $Bi_2Mo_2O_9$ (010) plane with oxygen positions.

mental surface area and density, the thickness of the β-phase overlayer at 4% excess Mo on Bi_2MoO_6 should be about 10 Å. Since NIRMS is confined to the outer layer (penetration depth < 5 Å), while XPS probes deeper ($15 \sim 40$ Å), this indicates that the catalyst seems to form either a thicker β-phase island on Bi_2MoO_6 or that the surface layer corresponds to a ratio of 1.5. In the latter case, the surface structure would be

$$Bi_2MoO_6 \xrightarrow{+Mo} (Bi_{1.57}Mo_{0.287}\phi_{0.143})(Mo_{0.857}Bi_{0.143})O_6.$$

The surface can be considered as a Bi_2MoO_6-surface with a number of "surface defects" such as Mo-cations and cation vacancies in the Bi_2O_2-layer and Bi ions in the MoO_2-layers. The defects may be either randomly distributed over the surface or ordered in $Bi_2Mo_2O_9$-like "surface domains". Here, however, we do not touch on which surface state is actually formed. The answer to this question would necessitate further investigations using, for example, XPS with ion etching or electron microscopic studies.

These data may be used to construct an "outline surface model". Indeed, one of the authors (*31*) had earlier proposed a model based on the assumption that Bi_2MoO_6 is an active catalyst. The surface was assumed to consist entirely of planes (010) perpendicular to the MoO_2- and Bi_2O_2-layers. We have given the proof that this particular plane in stoichiometric $Bi_2MoO_6(\gamma)$ cannot be active since the compound is not active at all and only becomes so by introducing extra Mo. Consequently, our active surface plane has to be derived from the (010) plane of $Bi_2Mo_2O_9(\beta)$. Figure 9 shows the formation of "surface domains (β)" supposed to be the active species, at the (101) plane of γ when excess Mo is introduced in γ. The process of removing oxygens from the top layer (Fig. 8c) has been performed by discarding one out of every two equivalent oxygens. The surface model shows that the olefin adsorption site (B-site) in the MoO_2-layer discussed earlier (*31*) still exists in the "surface domains". It has been shown that the adsorption parameters for but-1-ene both on stoichiometric and Mo-enriched active γ are similar (see Table 1). Also, we assumed an active oxygen (O_A) should be located at the edge of the Bi_2O_2 plane in $Bi_2MoO_6(\gamma)$ (*31*). For the Bi_2O_2 layer we see that the layer is formed from alternating vacancies and oxygens, each vacancy and oxygen belonging to a pair of Bi cations. Some oxygens of the "surface domains" are only connected with one Bi-cation; the other site is empty. This type of oxygen should be active and form O_A. Correlation between activity and the maximum volume of strong butadiene adsorption (V_m) which relates to O_A is shown in Fig. 10. It seems clear that the formation of cation vacancies in

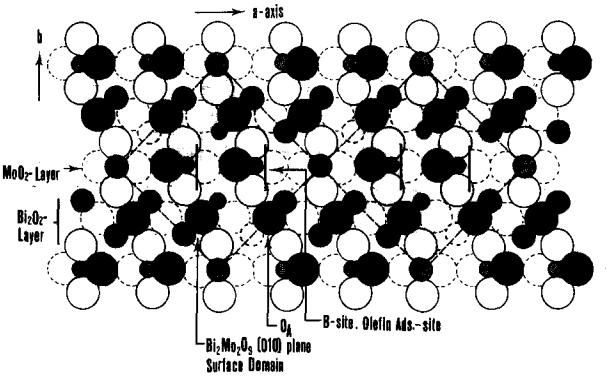

FIG. 9. Surface model of "surface domains" at the Bi_2MoO_6 (101) plane.

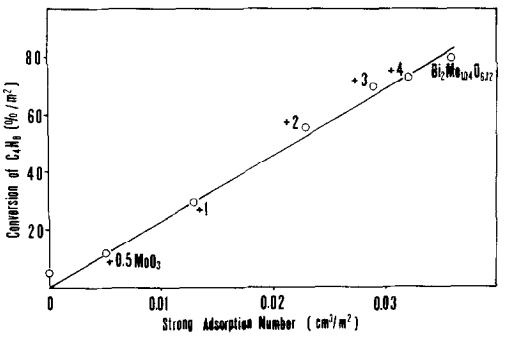

FIG. 10. Dependence of catalytic activity on the maximum volumes of strong butadiene adsorption (V_m) related to O_A on "impregnated" samples.

$Bi_2MoO_6(\gamma)$ with addition of Mo makes the catalyst active.

The postulate that only $Bi_2Mo_2O_9(\beta)$ is the active component agrees with the theory of Sleight and Linn (*32*) that a necessary feature of an active catalyst is the presence of cation vacancies in sites normally occupied by Bi^{3+} as given in the molecular formula $Bi^{I}(Bi_3^{II}\phi_c^{II}O_2)(Mo_4O_{16})$. If Bi^{I} is allowed to move over to the cation vacancy, we obtain $\phi_c^{I}(Bi_4^{II}O_2)(Mo_4O_{16})$. The I position would result in a situation entirely similar to that postulated by Sleight and Linn (*32*) to occur when $PbMoO_4$ is doped with Bi^{3+}. Another possibility for randomly occurring vacancies can be frequent twinning of $Bi_2Mo_2O_9$ crystals.

Our above conclusions rest on a combination of measurements concerning activity, adsorption, XPS and optical spectroscopic information. They are only strictly valid for samples very near the Bi/Mo = 2 edge for Bi_2MoO_6. For the majority of the "multiphase" samples in the entire range $2/3 \leq Bi/Mo \leq 2/1$, we have only the XPS data, the $Bi/Mo \approx 1$ value being indicative of the presence of a surface layer of the corresponding composition. Spectroscopic information ceases to be applicable because of the simultaneous presence of the γ- and α-phases, causing the ir and Raman spectra to become so complicated that identification of a separate surface layer becomes nearly impossible. Therefore, the presence of another type of surface layer with a composition $Bi/Mo \approx 1$ cannot be entirely excluded in the $2/3 \leq Bi/Mo \leq 2/1$ range, although it is believed to be improbable.

ACKNOWLEDGMENTS

We are indebted to Ir. E. Strijks and Ir. J. W. Wilms for the measurements of the Raman spectra, to Dr. G. Sawatzky and Ir. A. Heers at the University of Groningen for the measurements of XPS spectra and to Professor H. H. Brongersma for the NIRMS data. We thank Professor G. C. A. Schuit for many helpful discussions.

REFERENCES

1. Batist, Ph.A., Lippens, B. C., and Schuit, G. C. A., *J. Catal.* **5**, 55 (1966).
2. Batist, Ph.A., der Kinderen, A. H. W. M., Leeuwenburg, Y., Metz, F. A. M. G., and Schuit, G. C. A., *J. Catal.* **12**, 45 (1968).
3. Aykan, K., *J. Catal.* **12**, 281 (1968).
4. Boutry, P., Montarnal, R., and Wrzyszcz, J., *J. Catal.* **13**, 75 (1969).
5. Kolchin, I. K., Bobkov, S. S., and Margolis, L.Ya., *Neftekhimia* **4**(2), 301 (1964).
6. Batist, Ph.A., Bouwens, J. F. H., and Schuit, G. C. A., *J. Catal.* **25**, 1 (1972).
7. Erman, L.Ya., and Galperin, E. L., *Zh. Neorg. Khim.* **13**, 927 (1968).
8. Erman, L.Ya., and Galperin, E. L., *Russ. J. Inorg. Chem.* **15**, 441 (1970).
9. Cesari, M., Perego, G., Zazzetta, A., Manara, G., and Notari, B., *J. Inorg. Nucl. Chem.* **33**, 3595 (1971).
10. Batist, Ph.A., Prette, H. J., and Schuit, G. C. A., *J. Catal.* **15**, 281 (1969).
11. Matsuura, I., and Schuit, G. C. A., *J. Catal.* **20**, 19 (1971).
12. Carter, W. J., Schweitzer, G. K., Carlson, A., and Thomas, J. *Electron Spectrosc. Relat. Phenom.* **5**, 827 (1974).
13. Scofield, J. H., Lawrence Livermore Laboratory Report UCRL-51326 (1973).
14. Notermann, T., Keulks, G. W., Skliarov, A., Maximov, Yu., Margolis, L.Ya., and Krylov, O. V., *J. Catal.* **39**, 286 (1975).
15. Trifirò, F., Hoser, H., and Scarle, R. D., *J. Catal.* **25**, 12 (1972).
16. Van den Elzen, A. F., and Rieck, G. D., *Acta Crystallogr.* **B29**, 2433 (1973).
17. Van den Elzen, A. F., and Rieck, G. D., *Acta Crystallogr.* **B29**, 2436 (1973).
18. Van den Elzen, A. F., and Rieck, G. D., *Mater. Res. Bull.* **10**, 1163 (1975).
19. Busey, R. H., and Keller, O. L., Jr., *J. Chem. Phys.* **41**, 215 (1964).

20. Leciejewicz, J., *Z. Kristallogr.* **121,** 158 (1965).
21. Tarte, P., and Liegeois-Duyckaerts, M., *Spectrochim. Acta* **28a,** 2029, 2037 (1972).
22. Bonnaire, R., *Compt Rend. Ser. B* **266,** 1415 (1968).
23. Hulett, L. G., and Thornton, D. A., *J. Inorg. Nucl. Chem.* **35,** 2661 (1973).
24. Cotton, F. A., and Wing, R. M., *Inorg. Chem.* **4**(6), 867 (1965).
25. Bassile, L. J., Ferraro, J. R., Lobonville, P., and Wall, M. C., *Coord. Chem. Rev.* **11,** 21 (1973).
26. Bril, T. W., Ph.D. Thesis, University of Eindhoven, The Netherlands (1976).
27. Bril, T. W., and Vogel, D. L., "Extension Schachtschneider NCA Program," Proc. Fifth Int. Conf. Raman Spectra (Freiburg), p. 516 (1976).
28. Blasse, G., *J. Inorg. Nucl. Chem.* **28,** 1124 (1966).
29. Gryzbowska, B., Haber, J., and Komorek, J., *J. Catal.* **25,** 23 (1972).
30. Mitchell, P. C. H., and Trifirò, F., *J. Chem. Soc. A,* 3138 (1970).
31. Matsuura, I., and Schuit, G. C. A., *J. Catal.* **25,** 314 (1972).
32. Sleight, A. W., and Linn, W. J., *Ann. N.Y. Acad. Sci.* **272,** 22 (1976).